Mendeleev Communications

Mendeleev Commun., 2026, **36**, 101–103

CO_2 hydrogenation over catalysts based on Fe–Co double complex salts

Alevtina N. Gosteva,*[a] Mayya V. Kulikova,[b] Sergey A. Sviderskiy,[b] Alena A. Grabchak,[b] Semen E. Lapuk[c] and Alexander V. Gerasimov[c]

[a] *I. V. Tananaev Institute of Chemistry, FRC Kola Science Centre of the Russian Academy of Sciences, 184209 Apatity, Murmansk Region, Russian Federation. E-mail: angosteva@list.ru*

[b] *A. V. Topchiev Institute of Petrochemical Synthesis, Russian Academy of Sciences, 119991 Moscow, Russian Federation*

[c] *Alexander Butlerov Institute of Chemistry, Kazan Federal University, 420008 Kazan, Russian Federation*

DOI: 10.71267/mencom.7786

A FeCo catalyst obtained by thermolysis of double complex salts (DCSs) was used for the selective hydrogenation of CO_2 to CH_4. The DCS-based catalyst did not require activation, and its structure remained unchanged either during high-temperature treatment with H_2 or CO or under the process conditions of CO_2 hydrogenation; therefore, the catalyst selectivity was not subject to structural changes.

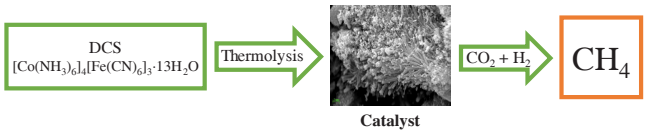

Keywords: bimetallic catalyst, catalysis, CO_2 hydrogenation, double complex salt, methane.

The need to reduce greenhouse gas emissions into the atmosphere has become urgent in recent decades. Research focus has shifted towards the chemical use of CO_2. The research on CO_2 hydrogenation is aimed at obtaining valuable C_{5+} hydrocarbons and oxygen-containing compounds. Methane is a by-product in such processes, which reduces the selectivity for target products. However, according to the new power-to-gas concept, methane can be considered as a target product, since it can be returned to the production cycle as a fuel.[1,2]

Dement'ev *et al.*[3] analyzed the main trends in the hydrogenation of CO_2 into methane; nickel-based catalysts were most commonly used for this process.[4–8] Another approach to the development of CO_2 methanation catalysts was to replace nickel as an active component with other metals such as Co and Fe.[9–13] Cobalt exhibits high methanation activity compared to that of other Group VIII metals,[9–12] but its disadvantage is a relatively low reaction rate of hydrogen conversion compared to nickel. However, high CO_2 conversion and almost 100% selectivity for methane formation were achieved in the presence of a cobalt-based catalyst.[11,13] In contrast to cobalt, iron[2,9] exhibits relatively high activity in the hydrogen-to-gas conversion reaction.[2,9] The idea of combining Fe and Co active centers in an iron–cobalt catalyst was implemented,[14–16] and the introduction of metallic Co increased CO_2 sorption and promoted the formation of active iron carbides, which favored the formation of C–C bonds characteristic of the iron carbide phase. The synergism of iron and cobalt in the composition of active centers was achieved by the formation of an active phase due to the thermal decomposition of iron and cobalt double complex salts (DCSs).[17,18] A methane-selective CO_2 hydrogenation catalyst based on a bimetallic iron–cobalt composition was obtained by thermolysis of DCSs.

The use of nonisothermal kinetics approaches is promising to optimize the process conditions for producing CO_2 methanation catalysts. According to IUPAC recommendations,[19–21] the determination of activation energy (E), pre-exponential factor (A), and reaction model (f) makes it possible to predict the behavior of a material over a wide temperature range.[22]

The goal of this work was to determine the structure of a methane-selective catalyst for CO_2 hydrogenation based on DCSs and to establish the relationship between the catalyst structure and activity and stability in the methanation reaction. The kinetic parameters of the thermolysis process and the choice of an optimal prognostic model for nonisothermal kinetics were of further interest.

The study of the kinetics of thermolysis for determining the kinetic parameters of decomposition made it possible to predict thermal stability in both dynamic and static modes of thermal destruction on a time scale corresponding to real technological processes. Therefore, the kinetic studies of stability are important from the point of view of further practical use of the proposed systems.

Four nonisothermal scans were performed to determine the kinetic parameters of the process of $[Co(NH_3)_6]_4[Fe(CN)_6]_3 \cdot 13H_2O$ (DCS 4/3) thermolysis according to ICTAC recommendations.[15,19–21] The samples were heated from 40 to 1000 °C at rates of 1, 5, 10 and 20 K min^{-1}. Figure S1 (see Online Supplementary Materials) shows the TG/DSC curves.

Thus, the optimal models and kinetic parameters of all stages of DCS decomposition were determined during the kinetic study of thermolysis. On this basis, we concluded that the decomposition was an autocatalytic process.

The DCS Co/Fe base central atom ratio was 1/1 in a previous work.[18] To increase the catalyst activity in methanation, this ratio was increased to 4/3. Both catalysts were obtained by thermolysis at 650 °C in an atmosphere of Ar. For example, a catalyst sample for the hydrogenation of CO_2 into methane was obtained by the destruction of DCS 4/3 and designated as DCS 4/3 MET (methane), and a catalyst for obtaining C_{5+} hydrocarbons[19] (a reference sample) was obtained by the destruction of DCS 1/1 and designated as DCS 1/1 HC (hydrocarbons). The composition of the samples determined by atomic absorption spectroscopy is presented in Table S4 (see Online Supplementary Materials). The specific surface areas and average pore sizes of DCS 4/3 MET and DCS 1/1 HC were 50.1 and 36.4 m^2 g^{-1} and 12.7 and 40.0 nm, respectively.

For a micrograph of DCS 4/3 MET, see Figure S4 (Online Supplementary Materials). The microscopy data for DCS 1/1 HC were reported elsewhere.[17]

Figure 1 shows the IR spectra of DCS 4/3 MET samples before and after activation and after CO_2 hydrogenation. It can be seen that neither the activation nor the hydrogenation had any effect on the IR spectra. The polyconjugation region (highlighted in Figure 1) has weak reflections, but the presence of polyconjugation bonds was significantly less than that observed for the catalysts described previously.[23] Therefore, it can be assumed that the interaction of a metal with carbon occurred mainly not in the areas of polyconjugation.

The X-ray diffraction patterns (Figure S5, Online Supplementary Materials) of DCS 4/3 MET samples before and after activation and after CO_2 hydrogenation also showed that the phase composition of the catalyst did not change significantly after the treatment and CO_2 hydrogenation processes.

The distinct peaks at around 1346 and 1586 cm^{-1} in the Raman spectra belong to the D band of disordered graphitic carbon and the G band arising from the stretching vibrations of C–C bonds in the plane of the graphite lattice.

Table 1 gives the results of catalytic tests of DCS 1/1 HC and DCS 4/3 MET catalysts. Gaseous reactants ($H_2 : CO_2 = 3 : 1$) were fed into the reactor at 2.0 MPa and a space velocity of 1500 h^{-1}.

The CO_2 conversion (X_{CO_2}) increased with temperature to close values of 26–27%, but selectivity changes were completely different. The main products of CO_2 hydrogenation on DCS 1/1 HC were C_{5+} hydrocarbons, and selectivity for these products decreased from 78 to 54%; the most significant by-product was CO (15–27%).

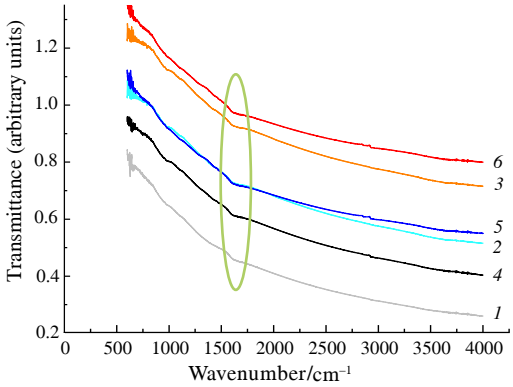

Figure 1 IR spectra of samples before [(*1*) nonactivated, (*2*) H_2-activated, and (*3*) CO-activated catalysts] and after CO_2 hydrogenation [(*4*) nonactivated, (*5*) H_2-activated, and (*6*) CO-activated catalysts]; O shows a polyconjugation area.

Table 1 Comparison of the main process characteristics of carbon dioxide hydrogenation on DCS 1/1 HC and DCS 4/3 MET catalysts.

T/°C	X_{CO_2} (%)	Selectivity (%)				$A^a \times 10^6$/ $mol_{CO_2}\ g_{Me}^{-1}\ s^{-1}$
		C_1	C_2–C_4	C_{5+}	CO	
DCS 1/1 HC						
230	12	5	2	78	15	1.8
250	14	7	3	73	17	1.4
270	18	11	4	62	23	2.5
290	21	14	4	55	27	3.7
310	26	17	4	54	25	4.6
DCS 4/3 MET						
230	5	83	4	10	3	0.7
250	9	71	11	11	7	1.2
270	16	65	13	12	10	2.2
290	22	58	14	16	12	2.9
310	27	56	16	15	13	3.6

[a] The specific activity–metal time yield (MTY) of a catalyst is the number of reacted moles of CO_2 per gram of Fe–Co per second.

The DCS 4/3 MET catalyst showed a predominance of CH_4 formation, and the selectivity for this product decreased from 83 to 56% with the temperature; C_{5+} hydrocarbons were the second most selective products (10–16%). They were slightly ahead of C_2–C_4 hydrocarbons (4–16%) and CO (3–13%). The formation of C_2–C_4 hydrocarbons on DCS 4/3 MET was significantly higher than that on DCS 1/1 HC: maximum selectivity values were 16 *vs.* 4%.

Figure 2 shows the temperature dependences of selectivity for C_{5+} hydrocarbons and methane for DCS 4/3 MET and DCS 1/1 HC. This dependence for DCS 1/1 HC was typical for FTS and CO_2 hydrogenation catalysts: the selectivity for C_{5+} hydrocarbons decreased, and the selectivity for methane increased with the process temperature. However, these dependences were opposite for the DCS 4/3 MET catalyst: when the process temperature increased, the selectivity for C_{5+} hydrocarbons increased, and the selectivity for methane decreased. Moreover, the selectivity values of DCS 4/3 MET for CH_4 were close to the selectivity for C_{5+} on DCS 1/1 HC at the same temperatures.

Thus, we found that changing the ratio between cobalt-containing and iron-containing components in the DCS composition in favor of the cobalt-containing component makes it possible to completely change the selectivity of the resulting catalyst and ensure the predominance of methane formation over the production of C_{5+} hydrocarbons. According to physical and chemical studies, the formation of an active phase was achieved, which was mainly represented by an alloy of iron and cobalt. An analysis of the X-ray diffraction patterns of the samples (Figure S5) showed that, in pre-activated DCS 1/1 HC and CO_2 used in hydrogenation without pre-activation, the iron–cobalt alloy formed during thermolysis partially converted into carbides and iron oxide, which were active in the formation of C_{5+} hydrocarbons. However, the only clearly identifiable crystalline phase in the DCS 4/3 MET sample was an iron–cobalt alloy, and the method of its activation was not important here. This iron–cobalt alloy was inactive in the formation of C_{5+} hydrocarbons. Thus, the predominance of cobalt over iron in the alloy composition increased its hydrogenation activity, and the immobilization of iron in the alloy structure prevented the formation of carbides, which are active in the synthesis of C_{5+} hydrocarbons. Iron in the alloy limited the growth of hydrogenation activity. On the one hand, this reduced the activity of the catalyst and, on the other hand, limited the effect of strong exothermicity of the hydrogenation reaction, overheating of the active centers, and coke formation caused by this phenomenon; as a result, the catalyst was deactivated. The resulting structure was characterized by high resistance to the components of the reaction atmosphere: hydrogen and carbon monoxide. This ensured the practical immutability of the phase composition of the catalyst and contributed to the stable maintenance of the selectivity index. This feature of structure formation differed fundamentally from that observed in catalysts of similar

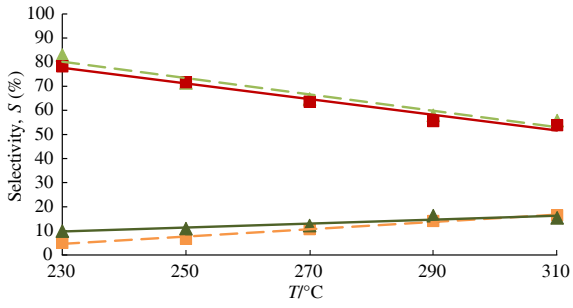

Figure 2 Dependences of catalysts selectivity for C_{5+} hydrocarbons and methane on process temperature : (▲) – $S_{C_{5+}}$, DCS 4/3 MET; (▲) – S_{CH_4}, DCS 4/3 MET; (■) – $S_{C_{5+}}$, DCS 1/1 HC; (■) – S_{CH_4}, DCS 1/1 HC.

composition obtained by the impregnation of individual iron and cobalt salts with nitric acid followed by heat treatment. In this case, the formation of an iron–cobalt alloy was also observed, but this alloy was almost completely converted into iron and cobalt carbides during the hydrogenation of CO_2. This increased the catalyst selectivity for C_{5+} hydrocarbons and reduced selectivity for methane.[16] This change occurred in a wide range of iron and cobalt ratios from 3 : 1 to 1 : 3, and an increase in the cobalt content did not prevent the decomposition of the alloy into carbides. Thus, thermolysis of DCSs as a method of catalyst preparation made it possible to create a highly stable structure of the active phase for the hydrogenation of CO_2 into methane.

Thus, the developed DCS-based catalyst does not require activation and its structure remains unchanged when treated with high-temperature hydrogen or carbon monoxide. In addition, there were no changes in the catalyst structure after CO_2 hydrogenation. Therefore, the catalyst was stable under the process conditions of CO_2 hydrogenation and its selectivity was not affected by structural changes characteristic of traditional CO and CO_2 hydrogenation catalysts.

This work was supported by the Russian Science Foundation, project no. 24-29-20076.

Online Supplementary Materials

Supplementary data associated with this article can be found in the online version at doi: 10.71267/mencom.7786.

References

1 S. Rönsch, J. Schneider, S. Matthischke, M. Schlüter, M. Götz, J. Lefebvre, P. Prabhakaran and S. Bajohr, *Fuel*, 2016, **166**, 276; https://doi.org/10.1016/j.fuel.2015.10.111.
2 M. Younas, L. Loong Kong, M. J. K. Bashir, H. Nadeem, A. Shehzad and S. Sethupathi, *Energy Fuels*, 2016, **30**, 8815; https://doi.org/10.1021/acs.energyfuels.6B01723.
3 K. I. Dement'ev, O. S. Dementeva, M. I. Ivantsov, M. V. Kulikova, M. V. Magomedova, A. L. Maximov, A. S. Lyadov, A. V. Starozhitskaya and M. V. Chudakova, *Pet. Chem.*, 2022, **62**, 445; https://doi.org/10.1134/S0965544122050012.
4 N. García-Moncada, J. C. Navarro, J. A. Odriozola, L. Lefferts and J. A. Faria, *Catal. Today*, 2022, **383**, 205; https://doi.org/10.1016/j.cattod.2021.02.014.
5 H. L. Huynh, W. M. Tucho and Z. Yu, *Green Energy Environ.*, 2020, **5**, 423; https://doi.org/10.1016/j.gee.2020.09.004.
6 X. Fang, L. Xia, S. Li, Z. Hong, M. Yang, X. Xu, J. Xu and X. Wang, *Fuel*, 2021, **293**, 120460; https://doi.org/10.1016/j.fuel.2021.120460.
7 R.-P. Ye, L. Liao, T. R. Reina, J. Liu, D. Chevella, Y. Jin, M. Fan and J. Liu, *Fuel*, 2021, **285**, 119151; https://doi.org/10.1016/j.fuel.2020.119151.
8 Z. Yan, Q. Liu, L. Liang and J. Ouyang, *J. CO2 Util.*, 2021, **47**, 101489; https://doi.org/10.1016/j.jcou.2021.101489.
9 I. Sreedhar, Y. Varun, S. A. Singh, A. Venugopal and B. M. Reddy, *Catal. Sci. Technol.*, 2019, **9**, 4478; https://doi.org/10.1039/C9CY01234F.
10 G. Weatherbee and C. H. Bartholomew, *J. Catal.*, 1984, **87**, 352; https://doi.org/10.1016/0021-9517(84)90196-9.
11 W. Li, X. Nie, X. Jiang, A. Zhang, F. Ding, M. Liu, Z. Liu, X. Guo and C. Song, *Appl. Catal., B*, 2018, **220**, 397; https://doi.org/10.1016/j.apcatb.2017.08.048.
12 W. Li, Y. Liu, M. Mu, F. Ding, Z. Liu, X. Guo and C. Song, *Appl. Catal., B*, 2019, **254**, 531; https://doi.org/10.1016/j.apcatb.2019.05.028.
13 G. Zhou, T. Wu, H. Xie and X. Zheng, *Int. J. Hydrogen Energy*, 2013, **38**, 10012; https://doi.org/10.1016/j.ijhydene.2013.05.130.
14 A. J. Markvoort, H. M. M. ten Eikelder, P. A. J. Hilbers, T. F. A. de Greef and E. W. Meijer, *Nat. Commun.*, 2011, **2**, 509; https://doi.org/10.1038/ncomms1517.
15 L. Guo, Y. Cui, P. Zhang, X. Peng, Y. Yoneyama, G. Yang and N. Tsubaki, *ChemistrySelect*, 2018, **3**, 13705; https://doi.org/10.1002/slct.201803335.
16 S. A. Svidersky, O. S. Dement'eva, M. I. Ivantsov, A. A. Grabchak, M. V. Kulikova and A. L. Maximov, *Pet. Chem.*, 2023, **63**, 443; https://doi.org/10.1134/S0965544123030234.
17 A. N. Gosteva, M. V. Kulikova, Y. P. Semushina, M. V. Chudakova, N. S. Tsvetov and V. V. Semushin, *Molecules*, 2021, **26**, 3782; https://doi.org/10.3390/molecules26133782.
18 A. N. Gosteva, M. V. Kulikova, M. I. Ivantsov, A. A. Grabchak, Y. P. Semushina, S. E. Lapuk, A. V. Gerasimov and N. S. Tsvetov, *Catalysts*, 2023, **13**, 1475; https://doi.org/10.3390/catal13121475.
19 S. Vyazovkin, A. K. Burnham, J. M. Criado, L. A. Pérez-Maqueda, C. Popescu and N. Sbirrazzuoli, *Thermochim. Acta*, 2011, **520**, 1; https://doi.org/10.1016/j.tca.2011.03.034.
20 N. Koga, S. Vyazovkin, A. K. Burnham, L. Favergeon, N. V. Muravyev, L. A. Pérez-Maqueda, C. Saggese and P. E. Sánchez-Jiménez, *Thermochim. Acta*, 2023, **719**, 179384; https://doi.org/10.1016/j.tca.2022.179384.
21 S. Vyazovkin, A. K. Burnham, L. Favergeon, N. Koga, E. Moukhina, L. A. Pérez-Maqueda and N. Sbirrazzuoli, *Thermochim. Acta*, 2020, **689**, 178597; https://doi.org/10.1016/j.tca.2020.178597.
22 A. Aghili, A. H. Shabani and V. Arabli, *Thermochim. Acta*, 2024, **740**, 179839; https://doi.org/10.1016/j.tca.2024.179839.
23 S. N. Khadzhiev, M. V. Kulikova, M. I. Ivantsov, L. M. Zemtsov, G. P. Karpacheva, D. G. Muratov, G. N. Bondarenko and N. V. Oknina, *Pet. Chem.*, 2016, **56**, 522; https://doi.org/10.1134/S0965544116060049.
24 B. Guo, G. Song, M. Chen, H. Yu, M. Ran, H. Wang, B. Yu, Z. Ma, J. Chen, M. Wang and X. Li, *Surf. Interfaces*, 2023, **42**, 103419; https://doi.org/10.1016/j.surfin.2023.103419.
25 B. Ma, R. D. Rodriguez, A. Ruban, S. Pavlov and E. Sheremet, *Phys. Chem. Chem. Phys.*, 2019, **21**, 10125; https://doi.org/10.1039/C9CP00093C.

Received: 1st April 2025; Com. 25/7786